Applied Clay Science 232 (2023) 106806

Contents lists available at ScienceDirect

Applied Clay Science

journal homepage: www.elsevier.com/locate/clay

Research Paper

Adsorption of methane and carbon dioxide by water-saturated clay minerals and clay rocks

Denys I. Grekov [a,*], Jean-Charles Robinet [b], Bernd Grambow [c]

[a] IMT Atlantique, GEPEA, UMR CNRS 6144, F-44307 Nantes, France
[b] Andra, R&D Division, Transfer Migration Group, 92298 Châtenay-Malabry, France
[c] SUBATECH, (IMT Atlantique, CNRS -IN2P3, Université de Nantes), F-44307 Nantes, France

ARTICLE INFO

Keywords:
CH_4
CO_2
Adsorption
Illite
Montmorillonite
Clay rock
Saturation

ABSTRACT

Understanding the effects of water on gas adsorption in geological media is of high importance in order to efficiently control numerous subsurface engineering process operating at gas/rock interfaces. Due to preferential interaction with clay surfaces, water fills their porous body, greatly reducing CH_4 and CO_2 adsorption capacity. In order to quantitatively describe CH_4 and CO_2 adsorption by hydrated clay minerals, this work proposes to rely on the mechanism of gas uptake by dissolution in pre-adsorbed pore water. This approach was employed to characterise water-saturated porous media of increasing complexity: mesoporous silica SBA-15 and silica gel with different pore sizes and geometry, isolated illite and montmorillonite and natural clay-rich rock (the Callovo-Oxfordian formation – COx, France) in powdered and crushed states. It was found that the solubility in water can reliably explain the CO_2 uptakes by hydrated pore systems regardless of their nature as well as the CH_4 uptakes, but only for solids with large mesopores and montmorillonite mineral. A so called "adsorption enhanced gas uptake in pore water" for CH_4, exceeding its solubility in bulk water by a factor of 5–8, was observed for the systems with narrow pore sizes, highlighting the impact of surface energy on gas uptake and the occurrence of the interaction of weakly-soluble methane with the surface, promoting its uptake in comparison to pure dissolution.

1. Introduction

Many geological gas reservoirs are natural subsurface rock formations with high surface area/void volume ratio, so they may enclose a significant part of trapped CH_4, CO_2 and other gases in adsorbed state. Clays are major mineral components of gas reservoirs, determining their porous structure and transport properties (Harrington and Horseman, 1999; Gensterblum et al., 2015). Multiscale/multiphysics understanding of these geological media is of prime importance to efficiently adapt deep engineering process, such as shale gas extraction, natural hydrogen recovery, geological gas storage or CO_2 sequestration (Benson and Cole, 2008; Busch et al., 2008; Plaat, 2009; Schaef et al., 2014; Cooper et al., 2016). Gas migration in clay-rocks are also deterministic for operation as well as safety assessments of geological radioactive waste disposal sites (Marschall et al., 2005). For instance, in these systems, at geological time scale, in addition to the release of gaseous hydrogen due to anaerobic corrosion of steel and reactive metals and to a much smaller degree due to water radiolysis, a significant part of gaseous organic degradation products or of ^{14}C-containing species may exist, depending on redox and pH conditions, in form of CH_4 or CO_2 (Grambow, 2016). Gas production processes are normally slow but it is possible that gas generation is faster than gas dissolution and migration through the engineered barrier components and the host rock, leading to desaturation of water saturated rock and diphasic gas flow in the repository and its near field.

Realistic assessment of the capacity of geological gas reservoirs and the migration of gas through natural barriers should rely not only on textural or geomechanical properties and composition of rock, but it should also take into account the effect of water which is omnipresent at near-saturation in many geological systems.

The mechanism of gas adsorption in presence of water is complex and strongly depends on the type of porous media, the amount of water it contains, pressure and temperature conditions. Since water is a polar molecule, it strongly and preferentially interacts with charged surface species, such as cations or hydroxyl groups, greatly reducing the number of available sites for the adsorption of other gases and vapours at the

* Corresponding author.
E-mail address: denys.grekov@imt-atlantique.fr (D.I. Grekov).

https://doi.org/10.1016/j.clay.2022.106806
Received 2 September 2022; Received in revised form 15 December 2022; Accepted 21 December 2022
Available online 3 January 2023

surface or inside micropores. For oxide systems, bearing significant amounts of polar surface species, the completion of pre-adsorbed water layers occurs at low relative humidity, greatly reducing the adsorption of CH_4 and CO_2 due to a "competition" effect (Kamimura and Endo, 2015; Tsujiguchi et al., 2016; AbdulKareem et al., 2018; Wang et al., 2020; Zhao et al., 2020). Under the same conditions, carbonaceous solids adsorb much lower amounts of water with the respect to their surface area, so that the process of CH_4 and CO_2 adsorption are almost unaffected by the effects of moisture at low and moderate relative humidity (Billemont et al., 2011, 2013; Tsujiguchi et al., 2016). In several specific cases, the presence of small amounts of water in the solid (at the initial stages of hydration) can albeit promote the adsorption of gases, due to the opening of the interlayer porosity in case of clays (Grekov et al., 2020b; Ziemiański et al., 2020) or modification of the energetics or the availability of adsorption sites in case of amphiphilic MOFs (Wang et al., 2017; Benoit et al., 2018) upon water uptake. For example, in case of smectite clays, the interlayer spaces are usually inaccessible for the incorporation of gases under fully-dehydrated conditions. At initial stages of water adsorption, the coordination of H_2O molecules to the charge-balancing cations results in expansion of the interlayer spaces, which makes them accessible for the diffusion of gases (Loring et al., 2012; Rother et al., 2013; Bowers et al., 2017, 2018, 2019; Loganathan et al., 2017, 2018; Schaef et al., 2017). It greatly increases CH_4 and CO_2 uptakes in comparison to completely dehydrated smectite clays, featuring the collapsed state of the interlayers and adsorbing gases mainly at external particle surfaces (Liu et al., 2013; Liang et al., 2016; Hwang and Pini, 2019; Grekov et al., 2020b; Du et al., 2020; Ziemiański et al., 2020).

Saturation with water of any porous media and of clay minerals in particular, usually results in lower capacities for gas uptake (except, perhaps the cases of gas hydrate formation) in comparison to fully dehydrated counterparts (Merkel et al., 2015a, 2015b; Li et al., 2016; Feng et al., 2018a). A number of studies carried out on shales, clay rocks, isolated clay minerals and coals, both in their dry state and equilibrated under different relative humidity (RH) conditions, revealed a progressive and usually linear decrease in CH_4 and CO_2 adsorption with increasing moisture content, until a threshold value, usually reached above 70% of RH. This is probably due to the filling of the smallest pores by water and hence the loss of an interconnected gas phase, strongly limiting the accessibility of gas to the overall pore network (Gensterblum et al., 2013; Merkel et al., 2015a, 2015b, 2016; Kadoura et al., 2016; Li et al., 2016; Feng et al., 2018a, 2018b). For pure clay phases, it is more related to the accessibility of surface due to presence of adsorbed water molecules. While several attempts were made to quantitatively interpret the reported trends, predictive models of gas adsorption in hydrated clay systems remain highly uncertain (Li et al., 2016; Feng et al., 2018b; Han et al., 2021). The uncertainty mainly comes from complex issues of the behaviour of gases in water confined inside nm-sized interparticle and charged interlayer (in case of smectites) pores, strong heterogeneity of clay minerals and lack of the understanding of gas transport and porous structure of hydrated geological systems (Holmboe et al., 2012; Massat et al., 2016).

According to recent experimental and molecular dynamics works, the uptakes of dissolved gases in liquid-filled nm-sized pores (S), are usually greater than given by gas solubility in bulk liquids (S°) under the same (P, T) conditions. The observed phenomenon, which refers to the effect of surface energy, was often termed "oversolubility" (Luzar and Bratko, 2005; Bratko and Luzar, 2008; Pera-Titus et al., 2009; Rakotovao et al., 2010; Clauzier et al., 2012; Ho et al., 2015; Coasne and Farrusseng, 2019; Liu et al., 2020). It is a complex phenomenon supposed to be due to the layering of water (solvent) molecules in the vicinity of the charged surface of pores of the solid, promoting the organization of the dissolved gas molecules and/or their interaction with pore wall indicating adsorption phenomena. In the present work the term "adsorption-enhanced gas uptake in pore water" is employed instead of "oversolubility". The apparent solubility enhancement factor $s \sim S/S^\circ$, was found to decrease with the increasing S° and to be higher for non-polar solvents (5–30) in comparison to polar ones, such as water, alcohols or halogenated hydrocarbons (1–7) (Pera-Titus et al., 2009; Rakotovao et al., 2010; Clauzier et al., 2012). Textural properties of porous solids figure among key factors influencing the observed solubility enhancement factor – S/S°. For instance, systems with high surface area/pore volume ratio, characteristic for narrow pores (typically with sizes ranging between 3 and 6 nm) seem to offer the highest observed S/S° ratios, as compared to larger pore sizes.

The main objective of the present study was to experimentally verify to which extent the solubility in bulk water can explain CH_4 and CO_2 uptake by clay minerals under water-saturation conditions (Gadikota et al., 2017). To address this question, adsorption isotherms were measured for a series of porous media of increasing complexity: model mesoporous silica, pure clay phases (montmorillonite and illite, with interlayers, which are either accessible or inaccessible for water/gases) and clay –rock samples, all equilibrated under controlled (97%) RH conditions. Measured adsorption capacities were calculated with the respect to the amounts of water contained in samples and directly compared to the solubility of CH_4 and CO_2 in bulk water under the same (P, T) conditions.

2. Materials and methods

2.1. Clays and porous silica

Davisil silica gel and SBA-15 mesoporous silica were supplied by Sigma Aldrich. Pure-phase montmorillonite (referred as Mt) was obtained from Na-bentonite Kunipia F, received from Kunimine industries. Mt. of Kunipia F mainly features the substitutions in octahedral layer, with the structural formula $(X(I)_{0.44})[Al_{1.56}Mg_{0.305}Fe_{0.1}][Si_{3.95}Al_{0.05}]O_{10}(OH)_2$, where the principal cationic species in the exchangeable domain (X(I)) is Na^+ (Suzuki et al., 2004). After dispersion in deionized water (5 g/l) the <2 μm fraction was extracted by centrifugation at 1000 rpm (170 g) and exchanged with Na by 24 h contact with 0.2 mol/l NaCl solution, 6 cycles of centrifugation at 20000 rpm (44,800 g) and washing in deionized water, final washing in methanol and drying of suspension at 50 °C. Illite du Puy (I) was received from BRGM (Orléans, France) in a Na-exchanged form (Gaboreau et al., 2016). After the dispersion in demineralized water under ultrasound (30 min), it was further purified from quartz by an elutriation procedure and exchanged with Na by following the same protocol as for montmorillonite. In contrast to Mt., I presents the substitutions in both tetrahedral and octahedral layers and its structural formula is: $(X(I)_{0.12}Ca_{0.01}Na_{0.01}K_{0.53})[Si_{3.55}Al_{0.45}][Al_{1.27}Fe(III)_{0.36}Mg_{0.44}]O_{10}(OH)_2$ (Bardot, 1998). According to (Bardot, 1998; Bradbury and Baeyens, 2009; Gaboreau et al., 2016), illite du Puy contain 5–10% of smectite phases. The core samples of a natural clay-rock used come from the Callovo-Oxfordian (COx) mudstones, East of Paris basin, France (Gaucher et al., 2004). COx clay rock is mainly composed of clay minerals such as illite (I) and interstratified illite/smectite (I/S) phases, carbonates (C) and tectosilicates (T). Smectite fraction is mainly dominated by montmorillonite. Several depths were selected in order to analyse various clay fractions and I/S ratios. The mineralogical characteristics of the samples were reported in earlier works (Grekov et al., 2019, 2021; Grekov et al., 2020a) and are summarized in Table 1.

Clay samples were ground manually and sieved to collect a size fraction <100 μm. All the material was ground until it was smaller than 100 μm. Some COx clay rocks were crushed to the size of ~5–15 mm. Crushed and powdered samples are labelled "C" and "P" respectively. A part of prepared clays together with mesoporous silica were equilibrated at ≈ 97% of RH at 20 °C, inside a desiccator over saturated K_2SO_4 solution during 1 month.

Table 1
Simplified composition of clay samples.

Clay sample	Tectosilicates, %	Carbonates, %	Clay fraction	
			Content %	Simplified composition
Montmorillonite*	–	–	>95	Montmorillonite:
Illite du Puy	–	–	>95	Illite
COx-EST 48599 (−508,3 m)	20–30	25–35	40–50	Illite: 75–80% Smectite: 20–25%
COx-EST 48601 (−466 m)	20–30	25–30	40–50	Illite: 60–70% Smectite: 30–40%

* Extracted from bentonite Kunipia F.

2.2. CH_4 and CO_2 adsorption measurements

A manometric method was used for measurement of CH_4 and CO_2 adsorption isotherms at 20 °C and pressures ranging between P_{atm} and 8 MPa, following the methodology reported earlier (Grekov et al., 2020b; Grekov et al., 2021). The principle of the experimental setup is described in Appendix A. Samples for gas adsorption measurement are usually outgassed under dynamic vacuum and heating. However, in the present study, in order to preserve the hydrated structure of humidity-equilibrated solids, after being packed in measurement cell, powdered or ground samples of 5–8 g were purged with working gases 3 times and briefly (<30 s) evacuated to about 0.1 bar, to stay above water vapour saturation pressure at 20 °C for isotherm measurement. This protocol was validated by comparing hydrated sample weights before and after isotherm measurement; the weight variation did not exceed 1%. Note, that under given pressure conditions (up to 8 MPa), some of the H_2O molecules could be replaced by CO_2 or CH_4, thus being lost from the sample due to their transfer to the gas phase. Also, the observed weight loss could partially be explained by the sample's loss, due to sticking of the moist solid to the wall of adsorption measurement cell. In order to minimize an error propagation, the isotherms for hydrated solids were measured within two runs (of 3–4 points) on the same sample. CH_4 adsorption was measured before CO_2.

Isotherms were also collected for dehydrated clays and silica; those were outgassed at 170 °C for 24 h in an oven, rapidly transferred to the sample cell and further outgassed for another 24 h under dynamic vacuum, as reported in the previous works (Grekov et al., 2020b; Grekov et al., 2021). The dead volumes V_d of the sample holder, including free space in the sample cell, inter-particle voids and micro/mesoporous volume, were determined for dry and humidity-saturated solids by He expansion at different pressures (2–8 bar) within 4 runs. Measurement of the V_d at pressures above the atmospheric pressure allows to mitigate the error induced by H_2O vapour partial pressure in case of water-saturated samples.

2.3. Thermo-gravimetric analysis (TGA)

The measurements of water content in humidity-equilibrated solids were carried out with Setaram TG-DSC 111 thermo-gravimetric analyser. 5–20 mg of hydrated solid were heated in quartz crucibles from ambient temperature up to 800 °C under 20 ml/l of He flow. Temperature-induced weight variations were corrected by subtracting the TGA curves acquired for an empty crucible.

2.4. Textural analysis

External specific surface areas were determined from N_2 adsorption isotherms at −196 °C using the BET method by following the IUPAC recommendations (Thommes et al., 2015). The total porous volume was calculated from the amount of N_2 adsorbed at 0.95 $p/p°$. Pore sizes were determined from adsorption isotherms by applying the NLDFT (non-local density functional theory) model with the kernel for cylindrical pore for oxide surface (Maddox et al., 1997; Occelli et al., 2002, 2003). Adsorbed N_2 molecule cross section area at −196 °C used in the calculations was 0.162 nm^2.

Nitrogen adsorption isotherms were collected at relative pressure ranging between 10^{-5} and 1 using 3Flex automated static manometric adsorption analyser from Micromeritics. Before isotherm measurement, all samples were outgassed under dynamic secondary vacuum at 150 °C until residual pressure stabilization for at least 24 h. The volumes of cells unoccupied with the sample were determined at ambient temperature and at −196 °C by helium expansion.

3. Results and discussion

3.1. CH_4 and CO_2 adsorption by model porous silica

Among large number of works on the effects of moisture on gas physisorption, only a few studies refer to the systems at complete saturation with water at near-ambient temperature or above (Liu et al., 2013, 2020; Merkel et al., 2015a, 2016; Feng et al., 2018b). Thereby, in order to better understand the behaviour of CH_4 and CO_2 in nano-confined water, gas adsorption measurements on model porous systems saturated with water are required. Mesoporous silica SBA-15 and silica gel are suitable materials for such assays.

N_2 adsorption isotherms of SBA-15 and silica gel, shown in Fig. 1 (a), featured shape IV(a) according to the IUPAC classification (Thommes et al., 2015), confirming their mesoporous character, as usually reported

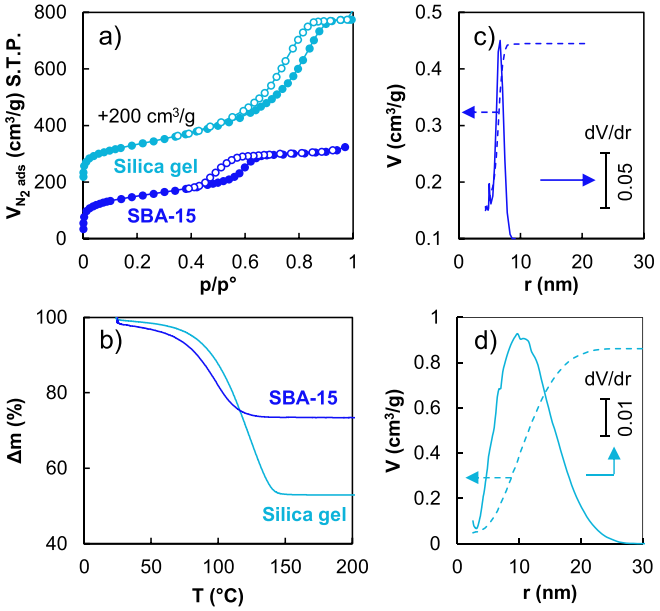

Fig. 1. (a) N_2 adsorption (filled symbols) and desorption (empty symbols) isotherms for SBA-15 (dark blue) and silica gel (ocean blue), (b) TGA curves (of humidity-saturated samples) and pore size distribution obtained using NLDFT for (c) SBA-15 and (d) silica gel. (For interpretation of the references to colour in this figure legend, the reader is referred to the web version of this article.)

for such materials (Thielemann et al., 2011; Cychosz et al., 2017; Kutarov and Schieferstein, 2019). For SBA-15, H1-type hysteresis between adsorption and desorption isotherms signified regular narrowly-distributed cylindrical pores, consistent with the synthesis route of this material. Large H2(b) hysteresis loop for silica gel, was indicative of ink-bottle pore geometry with the distribution of sizes of both, pore bodies and pore openings. This conclusion was supported by the results of pore size distribution analysis using the NLDFT method. Both mesoporous silica featured close values of the BET surface area (550 and 480 m^2/g for SBA-15 and silica gel respectively) but significantly differed in terms of pore volumes (0.42 and 0.87 cm^3/g respectively) and pore size distribution (6–8 and 6–20 nm respectively), Table 2. Thermogravimetric curves of humidity-saturated materials are represented in Fig. 1 (b). Weight loss of 27 and 47% before 150 °C for SBA-15 and silica gel, were assigned to the evaporation of capillary-condensed water and corresponded to 0.37 g/g and 0.88 g/g of water content with the respect of dry material. A good agreement between these values and mesopore volumes determined from N_2 adsorption, suggested a complete filling of pores with water at 97% of RH. The same conclusion was driven from a direct analysis of H_2O adsorption isotherms for such systems (Lin et al., 2018; Centineo et al., 2019).

CH_4 and CO_2 adsorption isotherms measured for both materials in dry and humidity-saturated states are represented in Fig. 2. The shape of methane adsorption isotherms for dehydrated silica is consistent with a monolayer formation on the pore surface. Higher adsorption capacity for SBA-15 in comparison to silica gel was due to its higher BET surface area. The adsorption isotherms of CO_2 featured a more complex shape with a progressively ascending component in the higher pressure range instead of a plateau, which could be due to polymolecular adsorption of subcritical at 20 °C CO_2. Both materials lost 80–90% of adsorption capacity under water-saturation conditions, which agrees with commonly observed trend (Kamimura and Endo, 2015; Merkel et al., 2015a, 2015b, 2016; Li et al., 2016; Feng et al., 2018a). Isotherms featured a linear shape. In order to verify to which extent one can consider the solubility of gases in pore water to explain gas uptakes, the adsorbed amounts of CH_4 and CO_2 were calculated with the respect of water content in materials and plotted against pressure, together with the solubility of these gases in bulk water at 20 °C (Diamond and Akinfiev, 2003; Duan and Mao, 2006), Fig. 2 (c).

According to the results in Fig. 2(c), in pressure range investigated herein (0.1–8 MPa), methane featured almost 10 times higher apparent solubility in water confined in SBA-15 mesopores in comparison to the bulk water. The same order of magnitude of the "oversolubility" was reported for similar systems studied earlier (Pera-Titus et al., 2009; Rakotovao et al., 2010; Clauzier et al., 2012). Regardless of the origins of enhanced gas uptake in nano-confined water as compared to bulk water (higher solubility of gas in ordered liquid adjacent to the surface or "attractive" interaction of the dissolved gas molecules with the pore wall, Fig. 2(d)), the surface area/pore volume ratio of the porous solid is the key factor controlling the process. Thus, in case of silica gel, which in contrast to SBA-15 featured lower surface area/pore volume ratio (550 m^2/cm^3 *vs.* 1310 m^2/cm^3) due to larger pore sizes, the measured amounts of adsorbed methane exceeded methane solubility in bulk water by only a factor of 1.8.

The same trend was observed for carbon dioxide, however adsorption-enhanced gas uptake in pore water was less significant and the adsorbed amounts only slightly exceeded the solubility of CO_2 in bulk water (factor of 1.3 for silica gel and 2.7 for SBA-15, Fig. 2 (c)).

Regarding linear domains of the isotherms, the uptake of CO_2 by dehydrated solids exceeded the uptake of CH_4 by a factor of 3–5, while in case of the dissolution of these gases in bulk water, this ratio was as high as 30 (in favour of CO_2, respective solubilises are $3.4{\cdot}10^{-5}$ and $1.25{\cdot}10^{-6}$ $mol{\cdot}cm^{-3}{\cdot}bar^{-1}$ at 20 °C) (Diamond and Akinfiev, 2003; Duan and Mao, 2006). Thereby, for the weakly soluble methane the interaction of the molecules with pore wall of water-saturated silica promotes the uptake, and for CO_2 the process is mainly controlled by dissolution. This conclusion is fully in line with the trends reported in the literature (Luzar and Bratko, 2005; Bratko and Luzar, 2008; Pera-Titus et al., 2009; Rakotovao et al., 2010; Clauzier et al., 2012; Ho et al., 2015; Coasne and Farrusseng, 2019; Liu et al., 2020).

Table 2
BET surface area, pore volume (from N_2 adsorption isotherm) and water content at 97% of RH at 20 °C of studied samples.

Material	S_{BET} (m^2/g)	$V_{p\ tot}$ (cm^3/g)	m_{H2O} ($g/g_{dry\ solid}$)
SBA-15	550	0.42	0.37
Silica gel	480	0.87	0.88
I	131	0.27	0.27
Mt	35	0.03	0.34
EST48599 (P)	38	0.05	0.06
EST48599 (C)	36	0.05	0.07
EST48601 (P)	31	0.03	0.05
EST48601 (C)	30	0.03	0.07

3.2. CH_4 and CO_2 adsorption by clay minerals and clay rocks

Illite and smectite phases as well as interstratified illite/smectite are frequently the principal constituents of many clay-rich rock formations, such as argillite. In contrast to illite, smectites have interlayers allowing exchange with the pore solutions. The low porosity of these formations is mainly associated to their clay fraction, so illite and smectite phases spatial distribution determines textural and fluid transport properties of rocks (Yven and Sammartino, 2007; Robinet et al., 2015; Song et al., 2015; Gaboreau et al., 2016). Various isolated phyllosilicate minerals, including mentioned clay phases, were extensively studied by high-pressure gas adsorption measurements (Giesting et al., 2012; Liu et al., 2013; Pini, 2014; Rexer et al., 2014; Pozo et al., 2017; Hwang and Pini, 2019; Hwang et al., 2019). At constant temperature, pressure and water content, the amounts of methane and carbon dioxide adsorbed by clay minerals depend on their specific surface area and on the accessibility of the interlayer spaces in case of smectites (Grekov et al., 2020b; Ziemiański et al., 2020; Hwang and Pini, 2021). The affinity of gas molecules to the clay surfaces correlates with the nature of exposed charge-balancing cations, structural charges and the shape of clay particles (Melnitchenko et al., 2000; Loganathan et al., 2020; Grekov et al., 2021).

While the sorption of CO_2 and CH_4 in dry state is mainly controlled by available surface area and remains rather clear concept, sorption of CO_2, accompanied by dissolution in pore water needs to be exposed to the same chemical constraints as any dissolved CO_2: formation of $CO_2(aq)$, H_2CO_3, HCO_3^- and CO_3^{2-} species, depending on pH conditions and CO_2 partial pressure. In order to assess the impact of clay rock pore water composition on CO_2 solubility and to account for the non-linear relation between CO_2 partial pressure and dissolved CO_2, geochemical modelling was conducted, using PHREEQC code (Parkhurst and Appelo, 2013). The pore water model of the Callovo-Oxfordian (Gaucher et al., 2006) clay rock was used to assess the impact of increased CO_2 pressure on pore water pH, ionic strength and CO_2 solubility in typical clay rock. This model accounts for mineral (calcite, illite, dolomite, quartz, pyrite, celestine, Fe chlorite) and ion exchange equilibria at 25 °C. The initial equilibrium partial pressure of CO_2 controlled by the mineral phase equilibria was calculated to be 10^{-2} bar, the pH was 7.21 and the ionic strength 0.11 $mol{\cdot}kg^{-1}$. Under these conditions 80% of the total dissolved CO_2 exists in form of HCO_3^-, 10% as CO_3^{2-} and only 10% as $CO_2(aq)$. At an imposed pressure of either 1 or 10 bar $CO_2(g)$ respectively, the pore water pH decreases to 6.06 or 5.48 and the total dissolved CO_2 becomes to 55% or 82% $CO_2(aq)$, approaching linearity between CO_2 pressure and dissolved CO_2 at high pressures. Caused by acidification of pore water and mineral dissolution, the ionic strength rises to either 0.14 or 0.18 $mol{\cdot}kg^{-1}$. However, the impact of slight ionic strength variation on gas solubility is low, so its effect is not taken into account. The results of simulation are shown in Fig. S1. The prevalence

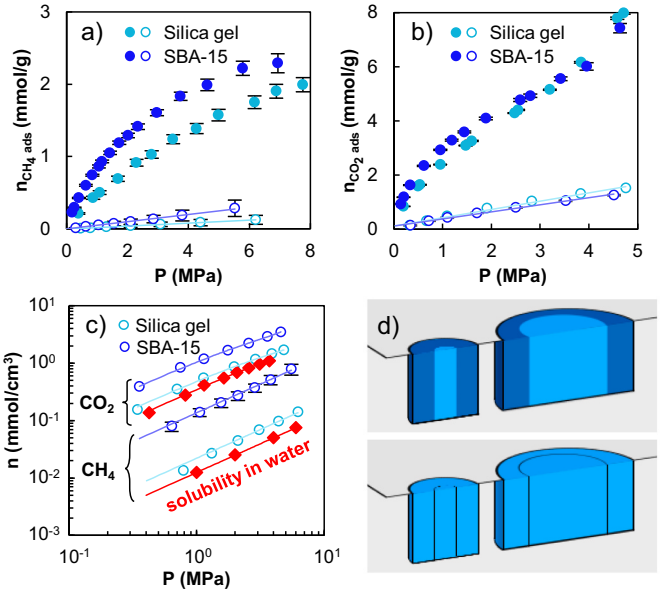

Fig. 2. CH_4 (a) and CO_2 (b) adsorption isotherms for SBA-15 (dark blue) and silica gel (ocean blue) under dehydrated (filled symbols) and water-saturated at 97% of RH (open symbols) states, (c) comparison of the solubility of CH_4 and CO_2 in water confined inside SBA-15 and silica gel pores and in bulk water (red lines) (Diamond and Akinfiev, 2003; Duan and Mao, 2006), (d) schematic illustration of the distribution of water states in nanopores filled with water: top – strongly-confined ordered pore water (dark blue) and weakly-confined bulk-like water (light blue), bottom – area of adsorption-enhanced interaction of dissolved gas molecules with pore wall. (For interpretation of the references to colour in this figure legend, the reader is referred to the web version of this article.)

of dissolved molecular CO_2 at elevated CO_2 pressures was also shown experimentally (Peng et al., 2013).

CH_4 and CO_2 adsorption isotherms for pure-phase illite and montmorillonite are represented in Fig. 3 (a), (b), (e), (f). Isotherms featured the same shape as in case of model mesoporous silica and the measured adsorption capacities under dehydrated conditions were in a good agreement with the results for similar montmorillonite and illite clays, with the respect to their BET surface areas (Ross and Marc Bustin, 2009;

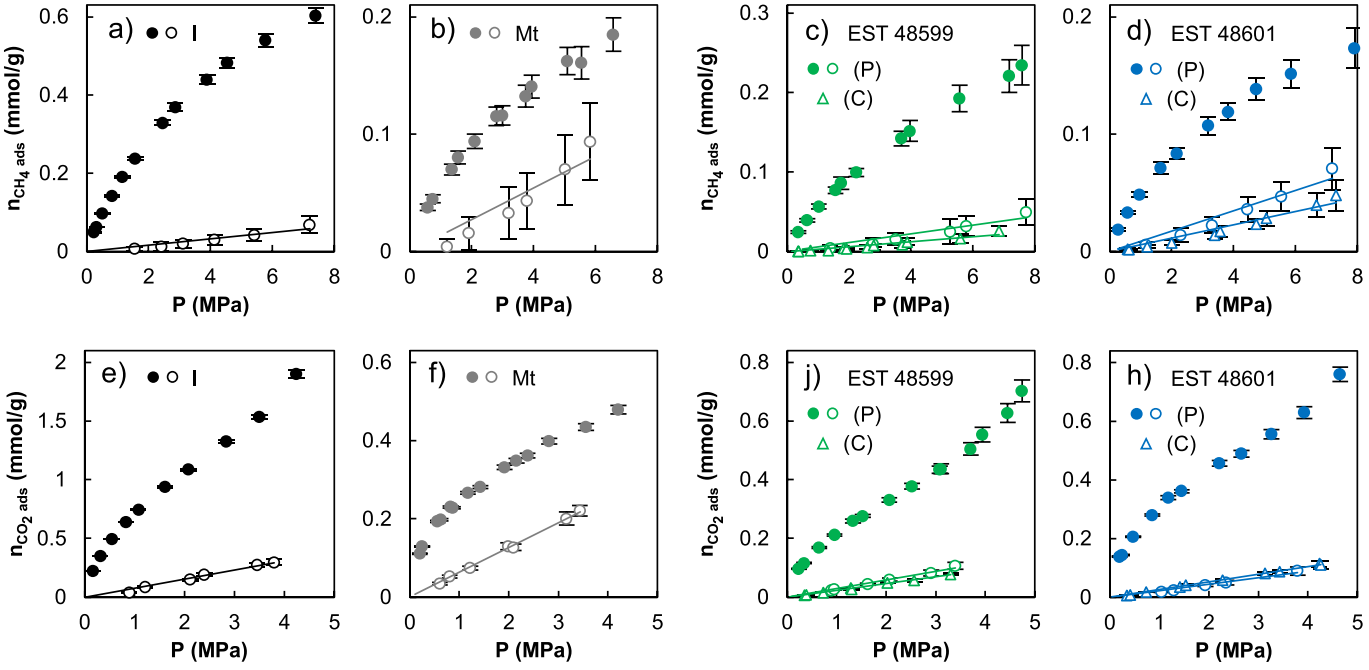

Fig. 3. Adsorption isotherms for CH_4 (figures a – d) and for CO_2 (figures e – h) for single-phase illite du Puy - I (a), (e) and montmorillonite - Mt. (b), (f) clays and for Callovo-Oxfordian clay rock samples EST 48599 (c), (j) and EST 48601 (d), (h) under dehydrated (filled symbols) and humidity-saturated (empty symbols) states. Triangles and circles correspond to crushed (C) and powdered (P) samples respectively. Gas adsorption isotherms by water-saturated clays are approximated by a line.

Liu et al., 2013; Jeon et al., 2014; Liang et al., 2016; Hwang and Pini, 2019; Hwang et al., 2019).

As expected, gas adsorption capacities dropped for both clay minerals under water-saturation conditions as compared to the dehydrated state. Gas adsorption isotherms by hydrated solids had rather linear shape. Montmorillonite loses by hydration about 50% of adsorption capacity for both gases, while illite – 80% and 90% for CO_2 and CH_4 respectively.

TGA curves allowed discerning two weight loss domains for hydrated clay minerals: before 150 °C, assigned to the evaporation of physisorbed water and above 500 °C, due to the dehydroxylation of the phyllosilicate structure, Fig. S3. Regarding the amounts of adsorbed CH_4 and CO_2 per total volume of water physisorbed at saturation, determined from the results of TGA (without distinguishing between interlayer and pore water in case of montmorillonite) (Ferrage et al., 2010; Ferrage, 2016; Grekov et al., 2019) one can realise that the solubility of gases in physisorbed water can reliably explain gas uptakes by both clay minerals, Fig. 4 (a) and (b). For I, which similarly to silica gel, features large mesopores (the closing of hysteresis loop between nitrogen adsorption/desorption isotherms at $p/p^\circ \sim 0.8$, Fig. S2), the absence of significant enhancement of CH_4 and CO_2 uptakes in comparison to the solubility of these gases in bulk water, could be explained by weak confinement effect of the capillary water due to low surface area/pore volume ratio, typical for large pore sizes. On the other hand, the origins of the same behaviour in case of montmorillonite were not entirely clear. Indeed, under saturation conditions, Mt. feature a significant fraction (about 50%) (Ferrage et al., 2010; Grekov et al., 2019) of strongly confined interlayer water and according to atomistic simulation works, are able to incorporate gases in the interlayer spaces (Gadikota et al., 2017). Considering a high confinement of the interlayer water, composed of 2–3 layers of organized H_2O molecules, in view of the foregoing, one should expect adsorption enhanced gas uptake in interlayer water in comparison to the solubility in bulk water.

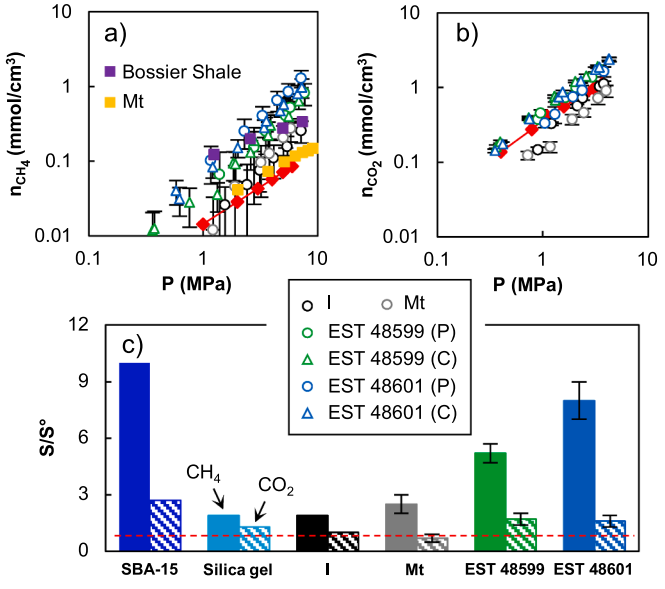

Fig. 4. Comparison of the solubility of CH_4 (a) and CO_2 (b) in water confined in pores of clay minerals and in bulk water (red symbols) (Diamond and Akinfiev, 2003; Duan and Mao, 2006). (c) Comparison of CH_4 and CO_2 adsorption-enhanced gas uptake in pore water (S) with the respect to their solubility in bulk water (S°) at 20 °C ($1.25 \cdot 10^{-6}$ and $3.4 \cdot 10^{-5}$ mol·cm^{-3}·bar^{-1} CH_4 and CO_2 respectively) for different porous solids. Violet and yellow squares correspond to CH_4 adsorption isotherms by water-saturated Bossier shale and montmorillonite from works of (Merkel et al., 2015a) and (Li et al., 2016). (For interpretation of the references to colour in this figure legend, the reader is referred to the web version of this article.)

Taking into account the prevalence of molecular form of dissolved CO_2 over HCO_3^- and CO_3^{2-} in clay pore water at pCO_2 pressures >1 bar and the impossibility of the two latter species to enter the interlayers at elevated carbon dioxide pressure, only CO_2 (major species of dissolved carbon dioxide) can enter the interlayer space of hydrated smectites (Loring et al., 2012, 2014; Schaef et al., 2012), depending on RH and possibly the type of interlayer cations. Thus, the observed picture for montmorillonite may signify the existence of two antagonistic effects upon gas uptake: on one side, the confinement of CH_4 and CO_2 molecules in hydrated interlayer space (Myshakin et al., 2013; Bowers et al., 2017; Gadikota et al., 2017) promoting the apparent adsorption-enhanced gas uptake, and on the other side, a high ionic force due to the presence of charge-balancing cations, suppressing gas uptake (Li et al., 2020). As shown by atomistic simulations, an increase of hydrated smectite interlayer distance results in a decrease of CO_2 solubility in the interlayer water (Botan et al., 2010) making it close to that in a bulk water under saturation conditions. According to (Botan et al., 2010; Gadikota et al., 2017), CO_2 uptake in the interlayer water (2 W and 3 W states) exceeds the solubility in bulk water by only a factor of 2–4.

Fig. 3 (c), (d), (j), (h) summarizes CH_4 and CO_2 adsorption isotherms for dry and humidity-saturated COx clay rock samples. It was illustrated that several properties of clay rocks, such as cation exchange capacity or retention of dissolved chemical species, related to phyllosilicate layer charge and illite/smectite ratio, can be described in "bottom-up" approach relying on the properties of pure-phase illite and montmorillonite (Tournassat et al., 2009). This concept cannot directly be employed today to describe the tendencies in gas physisorption, which, primarily depend on the textural properties of clay minerals. Even though, the impact of kerogens and other organic matter contents on CH_4 sorption might need to be considered as well.

Due to close values of the BET surface area, Table 2, humidity-saturated powdered and crushed argillite samples adsorbed similar quantities of CH_4 and CO_2. This observation was supported by the conclusion of the work (Robinet et al., 2012), which showed that COx size fraction <100 μm is representative of the bulk rock microstructure.

Within experimental error CO_2 uptakes by humidity-saturated COx clay rock (in terms of mmol/cm^3 of pre-adsorbed water) were close to CO_2 solubility in bulk water, Fig. 4. The measured volumetric uptakes did not significantly differ neither for the clay rock composition (Table 2) nor for the granulometry of the samples. It is worthy to be noticed that since at low pressure the CO_2 uptake in alkaline pore water is dominated by the formation HCO_3^- species, one may expect for COx clay rocks a higher CO_2 adsorption-enhanced uptake in thepore water at sub-atmospheric pressure range in comparison to a high pressure. This could not be concluded from the measurements performed far above 1 atm in the frame of this work. The data reported in Fig. 4 is also summarized in Table 3.

On the other hand, volumetric CH_4 uptakes by COx clay rock samples exceeded CH_4 solubility in bulk water by a factor of 5–8, which could be due to the effect of confinement in nanosized pores, by analogy with SBA-15. Combining the inputs from 3D FIB-SEM image reconstruction, mercury intrusion porosimetry, N_2 adsorption and recently from thermoporometry applied to water-saturated clays, it was reported that pores in the Callovo-Oxfordian clay rock typically range from the order of several nm to several dozens of nm (Yven and Sammartino, 2007; Song et al., 2015; Gaboreau et al., 2016; Grekov et al., 2019). Such narrow pore sizes in clay-rocks result from chemo-mechanical constrains

Table 3
The solubility of CH_4 and CO_2 in pore water of humidity-saturated solids with the respect to their solubility in bulk water (S/S°) according to (Diamond and Akinfiev, 2003; Duan and Mao, 2006.

	SBA-15	Silica gel	I	Mt	EST 48599	EST 48601
CH_4	10	1.9	1.9	2.5 ± 0.5	5.2 ± 0.5	8 ± 1
CO_2	2.7	1.3	1	0.7 ± 0.2	1.7 ± 0.3	1.6 ± 0.3

acquired during the diagenesis. They mainly originate from the mechanical compaction due to the lithostatic pressure and the precipitation of nm-sized mineral grains within the porosity. In case of isolated Mt., desagregated by ultrasound treatment in aqueous media during purification procedure, these constrains do not exist. Hence, upon swelling in moist atmosphere, the inter-granular pore sizes can be larger in comparison to COx clay rock. As a consequence, purified clay minerals and raw clay rock samples exhibited different pore sizes under the saturation conditions, so the enhancement of methane uptake in comparison to its solubility in bulk water was contrasted for these clay systems. Interestingly, EST 48601 sample featured slightly higher methane uptake in pore water than EST 48599 sample, which could be explained by narrower pores as suggested by its lower BET surface area / pore volume ratio (Table 2).

As demonstrated for shales of different maturity, CH_4 and CO_2 adsorption capacities positively correlate with the content of organic carbon (kerogen) in these systems (Ross and Marc Bustin, 2009; Gensterblum et al., 2013; Merkel et al., 2015a, 2015b; Hu and Mischo, 2020; Klewiah et al., 2020; Li et al., 2021). Due to hydrophobic character of kerogen, contented up to >20% in several shales, organic-rich formations adsorb less water than clay rocks, under saturation conditions, so their surfaces and pores remain more accessible for the adsorption of gases, presaging them with higher adsorption capacities than clay rock characterised by a low content of organic matter (Merkel et al., 2015a, 2016). It is thus important to exclude the effect of organic matter, to properly adapt the term of adsorption-enhanced gas uptake in pore water for raw natural clay rocks. In case of COx clay-rock, containing <2% of organic carbon (Gaucher et al., 2004), the effect of kerogen on CH_4 and CO_2 adsorption should not be significant (Merkel et al., 2015a, 2016). Methane adsorption data for humidity-saturated pure-phase montmorillonite (Li et al., 2016) and low-organic carbon Bossier shale (Merkel et al., 2015a) (content of kerogen close to that in COx) perfectly agreed with the trend reported in this study, Fig. 4 (a), indicating that the observed effect is not an artefact but a real consequence of adsorption-enhanced gas uptake in pore water. Consequently, in natural clay rock formations, the results from this study suggested that CH_4 and CO_2 adsorption-enhanced uptakes in pore water can be strongly contrasted, depending on clay rock mineralogy, their content of organic matter and their texture, influenced by geological history.

4. Conclusion

Predictive approach and quantitative interpreting of gas adsorption by hydrated porous media is challenging, especially in case of such complex porous systems as clay minerals or clay rocks. This work aimed at better understanding the features of CH_4 and CO_2 adsorption by clays saturated with water under controlled relative humidity conditions, assuming the mechanism of gas uptake by dissolution in clay water, as proposed earlier (Gadikota et al., 2017). The quantities of gases adsorbed per total amount of water in hydrated solids were directly compared with gas solubility in bulk water under the same (*P, T*) conditions. It was established that the solubility in water can reliably explain the CO_2 uptakes by hydrated porous media regardless of their nature. This observation is in line with relatively low "oversolubility" of CO_2 in nanoconfined liquids, as reported earlier (Pera-Titus et al., 2009; Rakotovao et al., 2010). Methane uptakes were properly described by dissolution as well, but only in case of solids with larger pores, where the confinement effects are not significant. On the other hand, in case of COx clay rocks, the adsorption-enhanced solubility of methane in pore water *vs.* bulk water (a ratio of 5–8) was observed, supposedly due to narrower pore sizes, in comparison to other systems, by analogy with SBA-15 silica. This finding potentially bears important consequences for industrial applications: both in case of shale gas behaviour and for radioactive waste disposal research, a higher "solubility" of methane in the pore space of very compact clay-rocks should be better considered in performance assessment.

Credit author statement

Denys I. Grekov: Conceptualization, Investigation, Methodology, Visualization, Writing - original draft, Writing - review and editing.

Jean-Charles Robinet: Resources, Validation, Writing - original draft.

Bernd Grambow: Funding acquisition, Supervision, Validation, Writing - original draft.

Declaration of Competing Interest

The authors declare that they have no known competing financial interests or personal relationships that could have appeared to influence the work reported in this paper.

Data availability

Data will be made available on request.

Acknowledgements

The present work was supported by the industrial chair "Storage and Disposal of Radioactive Waste" at IMT Atlantique, funded by ANDRA, Orano, and EDF.

Appendix A. Supplementary data

Supplementary data to this article can be found online at https://doi.org/10.1016/j.clay.2022.106806.

References

AbdulKareem, F.A., Mohd Shariff, A., Ullah, S., See, T.L., Keong, L.K., Mellon, N., 2018. Adsorption performance of 5A molecular sieve zeolite in water vapor–binary gas environment: experimental and modeling evaluation. J. Ind. Eng. Chem. 64, 173–187. https://doi.org/10.1016/j.jiec.2018.03.014.

Bardot, F., 1998. PhD Thesis: Surface Heterogeneity of Clay Minerals: Influence of Surface Compensating Cations of Illite on Gas Adsorption Mechanisms, pp. 1–206.

Benoit, V., Chanut, N., Pillai, R.S., Benzaqui, M., Beurroies, I., Devautour-Vinot, S., Serre, C., Steunou, N., Maurin, G., Llewellyn, P.L., 2018. A promising metal-organic framework (MOF), MIL-96(Al), for CO2 separation under humid conditions. J. Mater. Chem. A 6, 2081–2090. https://doi.org/10.1039/c7ta09696h.

Benson, S.M., Cole, D.R., 2008. CO2 sequestration in deep sedimentary formations. Elements 4, 325–331. https://doi.org/10.2113/gselements.4.5.325.

Billemont, P., Coasne, B., De Weireld, G., 2011. An experimental and molecular simulation study of the adsorption of carbon dioxide and methane in nanoporous carbons in the presence of water. Langmuir 27, 1015–1024. https://doi.org/10.1021/la103107t.

Billemont, P., Coasne, B., De Weireld, G., 2013. Adsorption of carbon dioxide, methane, and their mixtures in porous carbons: effect of surface chemistry, water content, and pore disorder. Langmuir 29, 3328–3338. https://doi.org/10.1021/la3048938.

Botan, A., Rotenberg, B., Marry, V., Turq, P., Noetinger, B., 2010. Carbon dioxide in montmorillonite clay hydrates: thermodynamics, structure, and transport from molecular simulation. J. Phys. Chem. C 114, 14962–14969. https://doi.org/10.1021/jp1043305.

Bowers, G.M., Todd Schaef, H., Loring, J.S., Hoyt, D.W., Burton, S.D., Walter, E.D., Kirkpatrick, J.R., 2017. Role of cations in CO2 adsorption, dynamics, and hydration in smectite clays under in situ supercritical CO2 conditions. J. Phys. Chem. C 121, 577–592. https://doi.org/10.1021/acs.jpcc.6b11542.

Bowers, G.M., Loring, J.S., Schaef, H.T., Walter, E.D., Burton, S.D., Hoyt, D.W., Cunniff, S.S., Loganathan, N., Kirkpatrick, R.J., 2018. Interaction of hydrocarbons with clays under reservoir conditions: in situ infrared and nuclear magnetic resonance spectroscopy and X-ray diffraction for expandable clays with variably wet supercritical methane. ACS Earth Sp. Chem. 2, 640–652. https://doi.org/10.1021/acsearthspacechem.8b00039.

Bowers, G.M., Loring, J.S., Walter, E.D., Burton, S.D., Bowden, M.E., Hoyt, D.W., Arey, B., Larsen, R.K., Kirkpatrick, R.J., 2019. Influence of smectite structure and hydration on supercritical methane binding and dynamics in smectite pores. J. Phys. Chem. C 123, 29231–29244. https://doi.org/10.1021/acs.jpcc.9b08875.

Bradbury, M.H., Baeyens, B., 2009. Sorption modelling on illite part I: titration measurements and the sorption of Ni, Co, Eu and Sn. Geochim. Cosmochim. Acta 73, 990–1003. https://doi.org/10.1016/j.gca.2008.11.017.

Bratko, D., Luzar, A., 2008. Attractive surface force in the presence of dissolved gas: a molecular approach. Langmuir 24, 1247–1253. https://doi.org/10.1021/la702328w.

Busch, A., Alles, S., Gensterblum, Y., Prinz, D., Dewhurst, D.N., Raven, M.D., Stanjek, H., Krooss, B.M., 2008. Carbon dioxide storage potential of shales. Int. J. Greenh. Gas Control 2, 297–308. https://doi.org/10.1016/j.ijggc.2008.03.003.

Centineo, A., Nguyen, H.G.T., Espinal, L., Horn, J.C., Brandani, S., 2019. An experimental and modelling study of water vapour adsorption on SBA-15. Microporous Mesoporous Mater. 282, 53–72. https://doi.org/10.1016/j.micromeso.2019.03.018.

Clauzier, S., Ho, L.N., Pera-Titus, M., Coasne, B., Farrusseng, D., 2012. Enhanced H 2 uptake in solvents confined in mesoporous metal-organic framework. J. Am. Chem. Soc. 134, 17369–17371. https://doi.org/10.1021/ja308157a.

Coasne, B., Farrusseng, D., 2019. Gas oversolubility in nanoconfined liquids: Review and perspectives for adsorbent design. Microporous Mesoporous Mater. 288, 109561. https://doi.org/10.1016/j.micromeso.2019.109561.

Cooper, J., Stamford, L., Azapagic, A., 2016. Shale Gas: a Review of the Economic, Environmental, and Social Sustainability. Energy Technol. 4, 772–792. https://doi.org/10.1002/ente.201500464.

Cychosz, K.A., Guillet-Nicolas, R., García-Martínez, J., Thommes, M., 2017. Recent advances in the textural characterization of hierarchically structured nanoporous materials. Chem. Soc. Rev. 46, 389–414. https://doi.org/10.1039/c6cs00391e.

Diamond, L.W., Akinfiev, N.N., 2003. Solubility of CO2 in water from −1.5 to 100°C and from 0.1 to 100 MPa: Evaluation of literature data and thermodynamic modelling. Fluid Phase Equilib. 208, 265–290. https://doi.org/10.1016/S0378-3812(03)00041-4.

Du, X., Guang, W., Cheng, Y., Hou, Z., Liu, Z., Yin, H., Huo, L., Lei, R., Shu, C., 2020. Thermodynamics analysis of the adsorption of CH4 and CO2 on montmorillonite. Appl. Clay Sci. 192, 105631. https://doi.org/10.1016/j.clay.2020.105631.

Duan, Z., Mao, S., 2006. A thermodynamic model for calculating methane solubility, density and gas phase composition of methane-bearing aqueous fluids from 273 to 523 K and from 1 to 2000 bar. Geochim. Cosmochim. Acta 70, 3369–3386. https://doi.org/10.1016/j.gca.2006.03.018.

Feng, D., Li, X., Wang, X., Li, J., Sun, F., Sun, Z., Zhang, T., Li, P., Chen, Y., Zhang, X., 2018a. Water adsorption and its impact on the pore structure characteristics of shale clay. Appl. Clay Sci. 155, 126–138. https://doi.org/10.1016/j.clay.2018.01.017.

Feng, D., Li, X., Wang, X., Li, J., Sun, F., Sun, Z., Zhang, T., Li, P., Chen, Y., Zhang, X., 2018b. Water adsorption and its impact on the pore structure characteristics of shale clay. Appl. Clay Sci. 155, 126–138. https://doi.org/10.1016/j.clay.2018.01.017.

Ferrage, E., 2016. Investigation of the interlayer organization of water and ions in smectite from the combined use of diffraction experiments and molecular simulations. A review of methodology, applications, and perspectives. Clay Clay Miner. 64, 348–373. https://doi.org/10.1346/CCMN.2016.0640401.

Ferrage, E., Lanson, B., Michot, L.J., Robert, J.L., 2010. Hydration properties and interlayer organization of water and ions in synthetic na-smectite with tetrahedral layer charge. Part 1. Results from X-ray diffraction profile modeling. J. Phys. Chem. C 114, 4515–4526. https://doi.org/10.1021/jp909860p.

Gaboreau, S., Robinet, J.C., Prêt, D., 2016. Optimization of pore-network characterization of a compacted clay material by TEM and FIB/SEM imaging. Microporous Mesoporous Mater. 224, 116–128. https://doi.org/10.1016/j.micromeso.2015.11.035.

Gadikota, G., Dazas, B., Rother, G., Cheshire, M.C., Bourg, I.C., 2017. Hydrophobic solvation of gases (CO2, CH4, H2, noble gases) in clay interlayer nanopores. J. Phys. Chem. C 121, 26539–26550. https://doi.org/10.1021/acs.jpcc.7b09768.

Gaucher, E., Robelin, C., Matray, J.M., Négrel, G., Gros, Y., Heitz, J.F., Vinsot, A., Rebours, H., Cassagnabère, A., Bouchet, A., 2004. ANDRA underground research laboratory: interpretation of the mineralogical and geochemical data acquired in the Callovian-Oxfordian formation by investigative drilling. Phys. Chem. Earth 29, 55–77. https://doi.org/10.1016/j.pce.2003.11.006.

Gaucher, É.C., Blanc, P., Bardot, F., Braibant, G., Buschaert, S., Crouzet, C., Gautier, A., Girard, J.P., Jacquot, E., Lassin, A., Negrel, G., Tournassat, C., Vinsot, A., Altmann, S., 2006. Modelling the porewater chemistry of the Callovian-Oxfordian formation at a regional scale. Compt. Rendus Geosci. 338, 917–930. https://doi.org/10.1016/j.crte.2006.06.002.

Gensterblum, Y., Merkel, A., Busch, A., Krooss, B.M., 2013. High-pressure CH4 and CO2 sorption isotherms as a function of coal maturity and the influence of moisture. Int. J. Coal Geol. 118, 45–57. https://doi.org/10.1016/j.coal.2013.07.024.

Gensterblum, Y., Ghanizadeh, A., Cuss, R.J., Amann-Hildenbrand, A., Krooss, B.M., Clarkson, C.R., Harrington, J.F., Zoback, M.D., 2015. Gas transport and storage capacity in shale gas reservoirs - a review. Part A: transport processes. J. Unconv. Oil Gas Resour. 12, 87–122. https://doi.org/10.1016/j.juogr.2015.08.001.

Giesting, P., Guggenheim, S., Koster van Groos, A.F., Busch, A., 2012. Interaction of carbon dioxide with Na-exchanged montmorillonite at pressures to 640bars: implications for CO 2 sequestration. Int. J. Greenh. Gas Control 8, 73–81. https://doi.org/10.1016/j.ijggc.2012.01.011.

Grambow, B., 2016. Geological disposal of radioactive waste in clay. Elements 12, 239–245. https://doi.org/10.2113/gselements.12.4.239.

Grekov, D., Montavon, G., Robinet, J.C., Grambow, B., 2019. Smectite fraction assessment in complex natural clay rocks from interlayer water content determined by thermogravimetric and thermoporometry analysis. J. Colloid Interface Sci. 555, 157–165. https://doi.org/10.1016/j.jcis.2019.07.076.

Grekov, D., Pré, P., Grambow, B., 2020a. On the use of manometry method for measurement of gas adsorption equilibria and characterization of clay texture with Derivative Isotherm Summation. Appl. Clay Sci. 184, 105372. https://doi.org/10.1016/j.clay.2019.105372.

Grekov, D.I., Suzuki-Muresan, T., Kalinichev, A.G., Pré, P., Grambow, B., 2020b. Thermodynamic data of adsorption reveal the entry of CH4 and CO2 in a smectite clay interlayer. Phys. Chem. Chem. Phys. 22, 16727–16733. https://doi.org/10.1039/d0cp02135k.

Grekov, D.I., Kalinichev, A.G., Suzuki-Muresan, T., Pré, P., Grambow, B., 2021. Direct experimental evidence of the effects of clay particles' basal-to-lateral surface ratio on methane and carbon dioxide adsorption. J. Phys. Chem. C 125, 11499–11507. https://doi.org/10.1021/acs.jpcc.1c00039.

Han, W., Li, A., Memon, A., Ma, M., 2021. Synergetic effect of water, temperature, and pressure on methane adsorption in shale gas reservoirs. ACS Omega. https://doi.org/10.1021/acsomega.0c05490.

Harrington, J.F., Horseman, S.T., 1999. Gas transport properties of clays and mudrocks. Geol. Soc. Spec. Publ. 158, 107–124. https://doi.org/10.1144/GSL.SP.1999.158.01.09.

Ho, L.N., Schuurman, Y., Farrusseng, D., Coasne, B., 2015. Solubility of gases in water confined in nanoporous materials: ZSM-5, MCM-41, and MIL-100. J. Phys. Chem. C 119, 21547–21554. https://doi.org/10.1021/acs.jpcc.5b06660.

Holmboe, M., Wold, S., Jonsson, M., 2012. Porosity investigation of compacted bentonite using XRD profile modeling. J. Contam. Hydrol. 128, 19–32. https://doi.org/10.1016/j.jconhyd.2011.10.005.

Hu, K., Mischo, H., 2020. Modeling high-pressure methane adsorption on shales with a simplified local density model. ACS Omega 5, 5048–5060. https://doi.org/10.1021/acsomega.9b03978.

Hwang, J., Pini, R., 2019. Supercritical CO2 and CH4 uptake by illite-smectite clay minerals. Environ. Sci. Technol. 53, 11588–11596. https://doi.org/10.1021/acs.est.9b03638.

Hwang, J., Pini, R., 2021. Enhanced sorption of supercritical CO 2 and CH 4 in the hydrated interlayer pores of smectite. Langmuir 37, 3778–3788. https://doi.org/10.1021/acs.langmuir.1c00375.

Hwang, J., Joss, L., Pini, R., 2019. Measuring and modelling supercritical adsorption of CO2 and CH4 on montmorillonite source clay. Microporous Mesoporous Mater. 273, 107–121. https://doi.org/10.1016/j.micromeso.2018.06.050.

Jeon, P.R., Choi, J., Yun, T.S., Lee, C.H., 2014. Sorption equilibrium and kinetics of CO2 on clay minerals from subcritical to supercritical conditions: CO2 sequestration at nanoscale interfaces. Chem. Eng. J. 255, 705–715. https://doi.org/10.1016/j.cej.2014.06.090.

Kadoura, A., Narayanan Nair, A.K., Sun, S., 2016. Adsorption of carbon dioxide, methane, and their mixture by montmorillonite in the presence of water. Microporous Mesoporous Mater. 225, 331–341. https://doi.org/10.1016/j.micromeso.2016.01.010.

Kamimura, Y., Endo, A., 2015. CO2 adsorption performance of mesoporous ceria with co-adsorbed water. Chem. Lett. 44, 1494–1496. https://doi.org/10.1246/cl.150687.

Klewiah, I., Berawala, D.S., Alexander Walker, H.C., Andersen, P., Nadeau, P.H., 2020. Review of experimental sorption studies of CO2 and CH4 in shales. J. Nat. Gas Sci. Eng. 73, 103045. https://doi.org/10.1016/j.jngse.2019.103045.

Kutarov, V.V., Schieferstein, E., 2019. Analytical equation for the mesopore size distribution function of open cylindrical capillaries. Adsorpt. Sci. Technol. 37, 468–479. https://doi.org/10.1177/0263617419846000.

Li, J., Li, X., Wang, X., Li, Y., Wu, K., Shi, J., Yang, L., Feng, D., Zhang, T., Yu, P., 2016. Water distribution characteristic and effect on methane adsorption capacity in shale clay. Int. J. Coal Geol. 159, 135–154. https://doi.org/10.1016/j.coal.2016.03.012.

Li, W., Nan, Y., You, Q., Jin, Z., 2020. CO2 solubility in brine in silica nanopores in relation to geological CO2 sequestration in tight formations: effect of salinity and pH. Chem. Eng. J. 127626 https://doi.org/10.1016/j.cej.2020.127626.

Li, W., Zhang, M., Nan, Y., Pang, W., Jin, Z., 2021. Molecular dynamics study on CO2 storage in water-filled kerogen nanopores in shale reservoirs: effects of kerogen maturity and pore size. Langmuir 37, 542–552. https://doi.org/10.1021/acs.langmuir.0c03232.

Liang, L., Xiong, J., Liu, X., Luo, D., 2016. An investigation into the thermodynamic characteristics of methane adsorption on different clay minerals. J. Nat. Gas Sci. Eng. 33, 1046–1055. https://doi.org/10.1016/j.jngse.2016.06.024.

Lin, Y., Horita, J., Abe, O., 2018. Adsorption isotope effects of water on mesoporous silica and alumina with implications for the land-vegetation-atmosphere system. Geochim. Cosmochim. Acta 223, 520–536. https://doi.org/10.1016/j.gca.2017.12.021.

Liu, D., Yuan, P., Liu, H., Li, T., Tan, D., Yuan, W., He, H., 2013. High-pressure adsorption of methane on montmorillonite, kaolinite and illite. Appl. Clay Sci. 85, 25–30. https://doi.org/10.1016/j.clay.2013.09.009.

Liu, C.C., Chou, H.J., Lin, C.Y., Janmanchi, D., Chung, P.W., Mou, C.Y., Yu, S.S.F., Chan, S.I., 2020. The oversolubility of methane gas in nano-confined water in nanoporous silica materials. Microporous Mesoporous Mater. 293, 109793. https://doi.org/10.1016/j.micromeso.2019.109793.

Loganathan, N., Yazaydin, A.O., Bowers, G.M., Kalinichev, A.G., Kirkpatrick, R.J., 2017. Molecular dynamics study of CO2 and H2O intercalation in smectite clays: effect of temperature and pressure on interlayer structure and dynamics in hectorite. J. Phys. Chem. C 121. https://doi.org/10.1021/acs.jpcc.7b06825.

Loganathan, N., Bowers, G.M., Yazaydin, A.O., Schaef, H.T., Loring, J.S., Kalinichev, A.G., Kirkpatrick, R.J., 2018. Clay swelling in dry supercritical carbon dioxide: effects of interlayer cations on the structure, dynamics, and energetics of CO2 intercalation probed by XRD, NMR, and GCMD simulations. J. Phys. Chem. C 122, 4391–4402. https://doi.org/10.1021/acs.jpcc.7b12270.

Loganathan, N., Yazaydin, A.O., Bowers, G.M., Ngouana-Wakou, B.F., Kalinichev, A.G., Kirkpatrick, R.J., 2020. Role of cations in the methane/carbon dioxide partitioning in nano- and mesopores of illite using constant reservoir composition molecular dynamics simulation. J. Phys. Chem. C 124, 2490–2500. https://doi.org/10.1021/acs.jpcc.9b10051.

Loring, J.S., Schaef, H.T., Turcu, R.V.F., Thompson, C.J., Miller, Q.R.S., Martin, P.F., Hu, J., Hoyt, D.W., Qafoku, O., Ilton, E.S., Felmy, A.R., Rosso, K.M., 2012. In situ molecular spectroscopic evidence for CO2 intercalation into montmorillonite in supercritical carbon dioxide. Langmuir 28, 7125–7128. https://doi.org/10.1021/la301136w.

Loring, J.S., Ilton, E.S., Thompson, C.J., Martin, P.F., Rosso, K.M., Felmy, A.R., Schaef, H.T., 2014. In situ study of CO2 and H2O partitioning between Na − montmorillonite

and variably wet supercritical carbon dioxide. Langmuir 30, 6120–6128. https://doi.org/10.1021/la500682t.
Luzar, A., Bratko, D., 2005. Gas solubility in hydrophobic confinement. J. Phys. Chem. B 109, 22545–22552. https://doi.org/10.1021/jp054545x.
Maddox, M.W., Olivier, J.P., Gubbins, K.E., 1997. Characterization of MCM-41 using molecular simulation: heterogeneity effects. Langmuir 13, 1737–1745. https://doi.org/10.1021/la961068o.
Marschall, P., Horseman, S., Gimmi, T., 2005. Characterisation of gas transport properties of the Opalinus clay, a potential host rock formation for radioactive waste disposal. Oil Gas Sci. Technol. 60, 121–139. https://doi.org/10.2516/ogst:2005008.
Massat, L., Cuisinier, O., Bihannic, I., Claret, F., Pelletier, M., Masrouri, F., Gaboreau, S., 2016. Swelling pressure development and inter-aggregate porosity evolution upon hydration of a compacted swelling clay. Appl. Clay Sci. 124–125, 197–210. https://doi.org/10.1016/j.clay.2016.01.002.
Melnitchenko, A., Thompson, J.G., Volzone, C., Ortiga, J., 2000. Selective gas adsorption by metal exchanged amorphous kaolinite derivatives. Appl. Clay Sci. 17, 35–53. https://doi.org/10.1016/S0169-1317(00)00003-X.
Merkel, A., Fink, R., Littke, R., 2015a. The role of pre-adsorbed water on methane sorption capacity of Bossier and Haynesville shales. Int. J. Coal Geol. 147–148, 1–8. https://doi.org/10.1016/j.coal.2015.06.003.
Merkel, A., Gensterblum, Y., Krooss, B.M., Amann, A., 2015b. Competitive sorption of CH4, CO2 and H2O on natural coals of different rank. Int. J. Coal Geol. 150–151, 181–192. https://doi.org/10.1016/j.coal.2015.09.006.
Merkel, A., Fink, R., Littke, R., 2016. High pressure methane sorption characteristics of lacustrine shales from the Midland Valley Basin, Scotland. Fuel 182, 361–372. https://doi.org/10.1016/j.fuel.2016.05.118.
Myshakin, E.M., Saidi, W.A., Romanov, V.N., Cygan, R.T., Jordan, K.D., 2013. Molecular dynamics simulations of carbon dioxide intercalation in hydrated Na-montmorillonite. J. Phys. Chem. C 117, 11028–11039. https://doi.org/10.1021/jp312589s.
Occelli, M.L., Olivier, J.P., Peridon-Melon, J.A., Auroux, A., 2002. Surface area, pore volume distribution, and acidity in mesoporous expanded clay catalysts from hybrid density functional theory (DFT) and adsorption microcalorimetry methods. Langmuir 18, 9816–9823. https://doi.org/10.1021/la020567o.
Occelli, M.L., Olivier, J.P., Petre, A., Auroux, A., 2003. Determination of pore size distribution, surface area, and acidity in fluid cracking catalysts (FCCS) from nonlocal density functional theoretical models of adsorption and from microcalorimetry methods. J. Phys. Chem. B 107, 4128–4136. https://doi.org/10.1021/jp022242m.
Parkhurst, D.L., Appelo, C.A.J., 2013. Description of Input and Examples for PHREEQC Version 3 — A Computer Program for Speciation, Batch-Reaction, One-Dimensional Transport, and Inverse Geochemical Calculations. U.S. Geological Survey Techniques and Methods, book 6, chapter A43, 497 p., U.S. Geological Survey Techniques and Methods, book 6, chapter A43.
Peng, C., Crawshaw, J.P., Maitland, G.C., Trusler, J.P.M., Vega-Maza, D., 2013. The pH of CO2-saturated water at temperatures between 308 K and 423 K at pressures up to 15 MPa. J. Supercrit. Fluids 82, 129–137. https://doi.org/10.1016/j.supflu.2013.07.001.
Pera-Titus, M., El-Chahal, R., Rakotovao, V., Daniel, C., Miachon, S., Dalmon, J.A., 2009. Direct volumetric measurement of gas oversolubility in nanoliquids: beyond Henry's law. ChemPhysChem 10, 2082–2089. https://doi.org/10.1002/cphc.200900058.
Pini, R., 2014. Assessing the adsorption properties of mudrocks for CO2 sequestration. Energy Procedia 63, 5556–5561. https://doi.org/10.1016/j.egypro.2014.11.589.
Plaat, H., 2009. Underground gas storage: why and how. Geol. Soc. Spec. Publ. 313, 25–37. https://doi.org/10.1144/SP313.4.
Pozo, M., Pino, D., Bessieres, D., 2017. Effect of thermal events on maturation and methane adsorption of Silurian black shales (Checa, Spain). Appl. Clay Sci. 136, 208–218. https://doi.org/10.1016/j.clay.2016.11.026.
Rakotovao, V., Ammar, R., Miachon, S., Pera-Titus, M., 2010. Influence of the mesoconfining solid on gas oversolubility in nanoliquids. Chem. Phys. Lett. 485, 299–303. https://doi.org/10.1016/j.cplett.2009.12.038.
Rexer, T.F., Mathia, E.J., Aplin, A.C., Thomas, K.M., 2014. High-pressure methane adsorption and characterization of pores in posidonia shales and isolated kerogens. Energy Fuel 28, 2886–2901. https://doi.org/10.1021/ef402466m.
Robinet, J.C., Sardini, P., Coelho, D., Parneix, J.C., Prt, D., Sammartino, S., Boller, E., Altmann, S., 2012. Effects of mineral distribution at mesoscopic scale on solute diffusion in a clay-rich rock: example of the Callovo-Oxfordian mudstone (Bure, France). Water Resour. Res. 48, 1–17. https://doi.org/10.1029/2011WR011352.
Robinet, J.C., Sardini, P., Siitari-Kauppi, M., Prêt, D., Yven, B., 2015. Upscaling the porosity of the Callovo-Oxfordian mudstone from the pore scale to the formation scale; insights from the 3H-PMMA autoradiography technique and SEM BSE imaging. Sediment. Geol. 321, 1–10. https://doi.org/10.1016/j.sedgeo.2015.02.007.
Ross, D.J.K., Marc Bustin, R., 2009. The importance of shale composition and pore structure upon gas storage potential of shale gas reservoirs. Mar. Pet. Geol. 26, 916–927. https://doi.org/10.1016/j.marpetgeo.2008.06.004.
Rother, G., Ilton, E.S., Wallacher, D., Hau, T., Schaef, H.T., Qafoku, O., Rosso, K.M., Felmy, A.R., Krukowski, E.G., Stack, A.G., Grimm, N., Bodnar, R.J., 2013. CO2 sorption to subsingle hydration layer montmorillonite clay studied by excess sorption and neutron diffraction measurements. Environ. Sci. Technol. 47, 205–211. https://doi.org/10.1021/es301382y.
Schaef, H.T., Ilton, E.S., Qafoku, O., Martin, P.F., Felmy, A.R., Rosso, K.M., 2012. In situ XRD study of Ca 2+ saturated montmorillonite (STX-1) exposed to anhydrous and wet supercritical carbon dioxide. Int. J. Greenh. Gas Control 6, 220–229. https://doi.org/10.1016/j.ijggc.2011.11.001.
Schaef, H.T., Davidson, C.L., Owen, A.T., Miller, Q.R.S., Loring, J.S., Thompson, C.J., Bacon, D.H., Glezakou, V.A., McGrail, B.P., 2014. CO2 utilization and storage in shale gas reservoirs: experimental results and economic impacts. Energy Procedia 63, 7844–7851. https://doi.org/10.1016/j.egypro.2014.11.819.
Schaef, H.T., Loganathan, N., Bowers, G.M., Kirkpatrick, R.J., Yazaydin, A.O., Burton, S.D., Hoyt, D.W., Thanthiriwatte, K.S., Dixon, D.A., McGrail, B.P., Rosso, K.M., Ilton, E.S., Loring, J.S., 2017. Tipping point for expansion of layered aluminosilicates in weakly polar solvents: supercritical CO2. ACS Appl. Mater. Interfaces 9, 36783–36791. https://doi.org/10.1021/acsami.7b10590.
Song, Y., Davy, C.A., Troadec, D., Blanchenet, A.M., Skoczylas, F., Talandier, J., Robinet, J.C., 2015. Multi-scale pore structure of COx claystone: towards the prediction of fluid transport. Mar. Pet. Geol. 65, 63–82. https://doi.org/10.1016/j.marpetgeo.2015.04.004.
Suzuki, S., Sato, H., Ishidera, T., Fujii, N., 2004. Study on anisotropy of effective diffusion coefficient and activation energy for deuterated water in compacted sodium bentonite. J. Contam. Hydrol. 68, 23–37. https://doi.org/10.1016/S0169-7722(03)00139-6.
Thielemann, J.P., Girgsdies, F., Schlögl, R., Hess, C., 2011. Pore structure and surface area of silica SBA-15: influence of washing and scale-up. Beilstein J. Nanotechnol. 2, 110–118. https://doi.org/10.3762/bjnano.2.13.
Thommes, M., Kaneko, K., Neimark, A.V., Olivier, J.P., Rodriguez-Reinoso, F., Rouquerol, J., Sing, K.S.W., 2015. Physisorption of gases, with special reference to the evaluation of surface area and pore size distribution (IUPAC Technical Report). Pure Appl. Chem. 87, 1051–1069. https://doi.org/10.1515/pac-2014-1117.
Tournassat, C., Gailhanou, H., Crouzet, C., Braibant, G., Gautier, A., Gaucher, E.C., 2009. Cation exchange selectivity coefficient values on smectite and mixed-layer illite/smectite minerals. Soil Sci. Soc. Am. J. 73, 928. https://doi.org/10.2136/sssaj2008.0285.
Tsujiguchi, T., Miyashita, Y., Osaka, Y., Kodama, A., 2016. Influence of contained water vapor on performance of simulated biogas separation by pressure swing adsorption. J. Chem. Eng. Jpn. 49, 251–256. https://doi.org/10.1252/jcej.14we283.
Wang, J., Wang, S., Xin, Q., Li, Y., 2017. Perspectives on water-facilitated CO2 capture materials. J. Mater. Chem. A 5, 6794–6816. https://doi.org/10.1039/c7ta01297g.
Wang, H., Yin, Y., Bai, J., Wang, S., 2020. Multi-factor study of the effects of a trace amount of water vapor on low concentration CO2 capture by 5A zeolite particles. RSC Adv. 10, 6503–6511. https://doi.org/10.1039/c9ra08334k.
Yven, B., Sammartino, S., 2007. Mineralogy, texture and porosity of Callovo-Oxfordian argillites of the Meuse/Haute-Marne region (eastern Paris Basin). Mém. Soc. Géol. Fr. 178, 73–90.
Zhao, J., Deng, S., Zhao, L., Yuan, X., Du, Z., Li, S., Chen, L., Wu, K., 2020. Understanding the effect of H2O on CO2 adsorption capture: mechanism explanation, quantitative approach and application. Sustain. Energy Fuel 4, 5970–5986. https://doi.org/10.1039/d0se01179g.
Ziemiański, P.P., Derkowski, A., Szczurowski, J., Kozieł, M., 2020. The structural versus textural control on the methane sorption capacity of clay minerals. Int. J. Coal Geol. 224, 103483. https://doi.org/10.1016/j.coal.2020.103483.